Fuel 89 (2010) 581–591

Contents lists available at ScienceDirect

Fuel

journal homepage: www.elsevier.com/locate/fuel

Numerical simulation of syngas combustion with a multi-spark ignition system in a diesel engine adapted to work at the Otto cycle

B. Gamiño *, J. Aguillón

Universidad Nacional Autónoma de México (UNAM), Instituto de Ingeniería, 04510, Coyoacán, Ciudad de México Distrito Federal, México

ARTICLE INFO

Article history:
Received 5 March 2009
Received in revised form 28 May 2009
Accepted 15 June 2009
Available online 9 July 2009

Keywords:
Combustion process simulation
Internal combustion engines
Syngas combustion
2D models
CFD PHOENICS

ABSTRACT

This work focuses on the construction of a 2D dynamic model, taking into consideration the turbulent flux combustion reactions of syngas inside a combustion chamber and its displacement through the cylinder of a diesel engine model OM 447 LA converted to Otto cycle operation. The engine has a multi-spark ignition system. The geometry of both the chamber and cylinder is symmetric to a radius of 0.064 m and to a length of 0.17595 m. The simulation is carried out on only half of the system, with a premixed supply of the syngas and air. The supply temperature of the mixture is 336 K. The supply relation air/syngas ratio is 1.1:1, and the supply pressure of the mixture is 1 bar. The gaseous phase is modeled as a multi-component mixture comprised of carbon monoxide (CO), hydrogen (H_2), methane (CH_4), nitrogen (N_2), carbon dioxide (CO_2) and oxygen (O_2). The study describes a Computational Fluid Dynamic (CFD) numerical model, in which the conservation of matter, motion and energy equations are solved; in addition, sub-models are used to represent the turbulence intensity and the multiple reactions. The model predicts the profiles of syngas speed, temperature, chemical composition, pressure, and turbulence intensity for the gases when the working parameters and the supply characteristics are modified (air–syngas ratio, initial temperature of the mixture, initial pressure, compression ratio, and engine speed). The equation formulation is elliptic staggered. The result is a simple nonlinear map that resolves combustion time sequences using the commercial code CFD in PHOENICS.

1. Introduction

Internal combustion engine (ICE) modeling is a multidisciplinary endeavor encompassing various areas, including thermodynamics, chemical kinetics, fluids mechanics, turbulence, heat transference, combustion, and numerical methods.

Although numerical models of the combustion of conventional fuels (e.g., natural gas, propane, gasoline and, diesel) in ICEs have been developed, few modeling and simulation studies have been performed on the syngas combustion process. Different authors have contributed to the development of a model that predicts the combustion process of conventional fuels, such as methanol, propane, gasoline, iso-octane, and methane, in spark ignition (SI) engines [1–8]. This model considers the process as starting with fuel ignition at the spark discharge, followed by the development of a small nucleus in the flame, which then grows and becomes a turbulent flame that travels through the engine combustion chamber and finally extinguishes next to the cylinder walls.

Abu-Nada et al. [9] investigated a theoretical model of the Otto cycle, with octane as the working fluid. This paper presents thermodynamic analysis of the SI engine. A theoretical model of the Otto cycle has been implemented. It is compared to those that use air as the working fluid with variable temperature specific heats. A wide range of engine parameters were studied, including the equivalence ratio, engine speed, maximum and outlet temperatures, brake mean effective pressure, gas pressure, and cycle thermal efficiency.

Several groups have developed a numerical model to predict the propagation of flames with homogeneous charges in SI engines [10–16]. This model solves the conservation of matter, motion, and energy equations using a sub-model to predict the burn rate. This model has been developed specifically to represent octane combustion and does not use a sub-model that includes the turbulence intensity, a characteristic of combustion phenomena.

In recent years, the dual-fuel combustion system has been proposed and studied but has not come into widespread use [17,18]. The conversion of a heavy-duty diesel engine to dual-fuel operation is discussed by Cordiner et al., who conducted numerical and experimental analyses of the combustion and exhaust emissions in a dual-fuel diesel/natural gas engine [19].

They performed experimental tests to define the engine performance, and reduce exhaust emissions, and used the resulting experimental data to develop a numerical model, characterized

* Corresponding author. Fax: +52 55 5616 2164.
E-mail address: benja_gamino@hotmail.com (B. Gamiño).

0016-2361/$ - see front matter © 2009 Elsevier Ltd. All rights reserved.
doi:10.1016/j.fuel.2009.06.030

Nomenclature

A y β	factors for the Arrhenius law
A_k	flame kernel surface area
C	concentration
C_p	specific heat at constant pressure
C_v	specific heat at constant volume
E_λ	activation energy
EP	rate of dissipation of energy
g	gravity vector
h	enthalpy
K	thermal conductivity coefficient
KE	turbulent kinetic energy
M	molecular mass
n_{spk}	number of spark
N	number of species
P	pressure
PRT(H)	prandt1 number
q	incoming energy per volume
Q_{spk}	energy spark
R	universal constant of gases
s	burning velocity
t	time
s_t	effective kernel growth speed
T	temperature
U	internal energy of the burned gas
v	speed
V_k^p	products stoichiometric coefficients
V_k^r	reagents stoichiometric coefficients
ω	chemical production rate
Y	mass fraction
ρ	density
λ	heat capacity
μ	dynamic viscosity
τ	tensions tensor
φ	external exhaust gas recycled fraction
Φ	fuel–air equivalence ratio

Subscripts

k	kernel
l	laminar
n	species n
t	turbulent
u	unburned

by a mixed one-dimensional (1D)-three-dimensional (3D) approach. A modified version of the KIVA-3 V code was used for the 3D simulation of the whole working cycle of the engine and to represent diesel injection and overall combustion [17].

Huang et al. [20] investigated the combustion characteristics of a direct-injection engine fueled with natural gas-hydrogen mixtures.

Saravanan and Nagarajan [21] conducted an experimental investigation on a Direct Injection (DI) dual fuel engine with hydrogen injection. In their study, hydrogen was injected in the intake manifold and diesel fuel was injected inside the engine cylinder in the conventional manner.

Several studies have indicated that hydrogen can be used as a sole fuel in the SI engine [22–26]. However, increasing the compression ratio in a SI engine would result in knocking. Hydrogen can be injected using either mechanical or electronic injectors. Electronic injectors allow greater control over the injection timing and injection duration, with quick response to operate under high-speed conditions.

Sridhar et al. [27] performed a zero-dimensional modeling study using a wrinkled flame theory for flame propagation to understand the in-cylinder pressure behavior with time in a reciprocating internal combustion engine.

They compared their findings with experimental data obtained using an engine operated on biomass derived from a mixture of producer gas and air. The required inputs for the laminar burning velocity and turbulence parameters were obtained from separate studies. The data related to laminar burning velocity for a producer gas/air mixture under thermodynamic conditions typical of an unburned mixture in an engine cylinder were obtained from one-dimensional flame calculations. The turbulence parameters were obtained by conducting a three-dimensional computational fluid dynamics study on a system with a bowl-in-piston geometry to simulate motored or non-firing conditions.

Only a few thermodynamic and 2D models have been developed to characterize the combustion process of multi-component fuels in internal combustion engines [28–31]. The model developed in the present work takes into consideration the multi-component nature of syngas (hydrogen, carbon monoxide, and methane), which is a product of the gasification of pinewood.

2. Description of the simulation model

2.1. Thermodynamic properties of air–syngas and combustion products

The specific heats of these species in syngas have different temperature dependencies. The specific heats of some species vary strongly with temperature, while those of other species are less temperature dependent.

The temperature-dependent specific heat for these species in syngas is calculated as

$$\frac{Cp}{R} = A + BT + CT^2 + DT^{-2} \tag{1}$$

where T is the temperature in Kelvin, and C_p and R have units of kJ/kmol K.

The values of the constants A, B, C, and D for the species are given in Table 1.

The specific heat for the air–syngas can be computed as

$$Cp_{mix} = Cp_a x_a + Cp_f x_f \tag{2}$$

The specific heat for the combustion products is calculated as

$$Cp_{mix} = \sum_{i=1}^{n} Cp_i x_i \tag{3}$$

where i stands for H_2, CO_2, CO, H_2O, O_2, and N_2. The mass fraction x^i is given as

Table 1
Coefficients used in Eq. (1).

Species	A	$B \times 10^3$	$C \times 10^6$	$D \times 10^5$
CH_4	1.702	9.081	2.164	0.000
CO	3.376	0.557	0.000	0.031
CO_2	5.457	1.045	0.000	1.157
H_2	3.249	0.422	0.000	0.083
N_2	3.280	0.593	0.000	0.040
O_2	3.639	0.506	0.000	0.227
H_2O	3.470	1.450	0.000	0.121

$$x_i = \frac{n_i M_i}{m_{mix}} \tag{4}$$

where m_{mix} is the total mass of the mixture, given as

$$m_{mix} = \sum_{i=1}^{n} n_i M_i \tag{5}$$

During combustion, a flame front is assumed to travel throughout the combustion chamber. The gases ahead of this flame are assumed to have the air–fuel mixture properties, whereas the gases behind it take the properties of the combustion products. Thus, it is very reasonable to estimate the specific heat for the mixture as follows

$$Cp_{mix} = Cp_{air-syngas}(1 - x_b) + Cp_{products}(x_b) \tag{6}$$

where x_{b} is evaluated from the Wiebe function and represents the burned fraction of the fuel.

2.2. General description

2.2.1. The syngas

The syngas used was obtained from the partial oxidation of pinewood, a process known as gasification [32]. The gas is made up of 36% combustible gases (carbon monoxide, hydrogen, and methane) and nitrogen and carbon dioxide (64%). The mean chemical composition of the syngas obtained experimentally from the gasification of pinewood in percentages by moles is CO, 25%; H_2, 6%; CH_4, 5%; CO_2, 11%; and N_2, 53% ($C_{0.1746}H_{0.2229}O_{0.0725}N_{0.5300}$).

During the syngas combustion process, the following homogeneous reactions are considered:

$$2CH_4 + O_2 \xrightarrow{K1} 4H_2 + 2CO \tag{A}$$

$$2CO + O_2 \xrightarrow{K2} 2CO_2 \tag{B}$$

$$2H_2 + O_2 \xrightarrow{K1} 2H_2O \tag{C}$$

Reaction (A) includes the formation of intermediate products that become reactants in reactions (B) and (C).

2.2.2. Internal combustion engine

The diesel engine model OM 447 LA is a heavy Mercedes Benz diesel engine. This engine was converted to operate only with syngas in the mechanical engineering laboratory at the University of Mexico (UNAM). To convert the engine from the diesel operation cycle to the Otto cycle, several adaptations were carried out. The most prominent modifications were as follows: modification of the cylinder head to hold the spark plugs and eliminate the diesel injection system, substitution of the valve holders, modification of the pistons to increase the volume of the combustion chamber from 122.7 cm^3 to 204.5 cm^3 (decreased compression ratio from 17.25 to 10.35), and implementation of an electronic starting system (incorporating the air supply system, the syngas supply system, as well as the implementation of pressure, temperature, speed, and oxygen sensors and the multi-spark ignition system).

2.3. Description of the model

Modeling in chemical kinetics and fluid dynamics is a central problem in the representation of homogeneous combustion mixtures (gases) inside the cylinders of ICEs not only because the system is reactive and turbulent but also because the reaction development is influenced by turbulent and flux-mixing fluctuations.

All methods for calculating the flux field when modeling the combustion process of reactive fluids in an ICE are based on the conservation of matter, motion, and energy equations [33]. Additionally, a mathematical model is included to represent the turbulence intensity, the multiple reactions and the thermal equation of state that links pressure, density, and temperature. Consequently, the equations governing an ideal homogeneous mixture of three reactive gas species (H_2, CO, and CH_4) are as follows:

Conservation of mass

$$\frac{\partial \rho}{\partial t} + \frac{\partial(\rho r v_r)}{r\partial r} + \frac{\partial(\rho v_z)}{\partial z} = 0 \tag{7}$$

Conservation of species

$$\frac{\partial(\rho Y_n)}{\partial t} + \frac{\partial(\rho r v_r Y_n)}{r\partial r} + \frac{\partial(\rho v_z Y_n)}{\partial z} = R_n \ (n = 1, 2, \ldots N) \tag{8}$$

$$R_n = M_n \omega_n \tag{9}$$

$$M_n \omega_n = \sum_{n=1}^{n=N} \left[A T^{\beta} \exp\left(-\frac{E_{\lambda}}{RT}\right) \right] (V_n^p - V_n^r) \prod_{n=1}^{n=N} C_n^{V_n^r} \tag{10}$$

$$C_n = \frac{\rho_n}{M_n} = \frac{\rho Y_n}{M_n} \tag{11}$$

Momentum conservation

In tensile notation

For component r

$$\frac{\partial(\rho v_r)}{\partial t} + v_r \frac{\partial(\rho v_r)}{\partial r} + v_z \frac{\partial v_r}{\partial z} = -\frac{\partial P}{\partial r} - \frac{1}{r}\frac{\partial(r\tau_{rr})}{\partial r} - \frac{\partial \tau_{rz}}{\partial z} \tag{12}$$

For component z

$$\frac{\partial(\rho v_z)}{\partial t} + v_r \frac{\partial(\rho v_z)}{\partial r} + v_z \frac{\partial v_z}{\partial z} = -\frac{\partial P}{\partial z} - \frac{1}{r}\frac{\partial(r\tau_{rz})}{\partial r} - \frac{\partial \tau_{zz}}{\partial z} \tag{13}$$

in which τ_{rr}, τ_{rz} and τ_{zz} are

$$\tau_{rr} = -\mu\left[2\frac{\partial v_r}{\partial r} - \frac{2}{3}(\nabla . v)\right] \tag{14}$$

$$\tau_{rz} = -\mu\left[2\frac{\partial v_z}{\partial r} + \frac{\partial v_r}{\partial z}\right] \tag{15}$$

$$\tau_{zz} = -\mu\left[2\frac{\partial v_z}{\partial z} - \frac{2}{3}(\nabla . v)\right] \tag{16}$$

$$(\nabla . v) = \frac{1}{r}\frac{\partial}{\partial r}(r v_r) + \frac{\partial v_z}{\partial z} \tag{17}$$

Conservation of energy

$$\begin{aligned} \rho C v \left(\frac{\partial T}{\partial t} + v_r \frac{\partial T}{\partial r} + v_z \frac{\partial T}{\partial z}\right) &= -\left[\frac{1}{r}\frac{\partial}{\partial r}(r q_r) + \frac{\partial q_z}{\partial z}\right] - T\left(\frac{\partial P}{\partial T}\right)\left(\frac{1}{r}\frac{\partial}{\partial r}(r v_r) + \frac{\partial v_z}{\partial z}\right) \\ &\quad - \left[\tau_{rr}\frac{\partial v_r}{\partial r} + \tau_{rz}\frac{\partial v_z}{\partial z} - \tau_{rz}\left(\frac{\partial v_z}{\partial r} + \frac{\partial v_r}{\partial z}\right)\right] \end{aligned} \tag{18}$$

Thermal equation of state

$$p = \rho R T \sum_{n=1}^{N} \left(\frac{Y^n}{M^n}\right) \tag{19}$$

Enthalpy

$$h_n = h_n^o + \int_{T^0}^{T} Cp^n dT \ (n = 1, 2, \ldots N) \tag{20}$$

Turbulence

In the present work, the turbulence is characterized by local values and is determined from modeled turbulent kinetic energy (KE) and turbulent kinetic energy dissipation rate (EP) transport equations [34–41]. Reynolds stresses are calculated using a gradient transport assumption, with an eddy viscosity that is a function of KE and EP. These assumptions are most appropriate in systems for which the production and dissipation of turbulence are close to equilibrium. In its simplest form, the model involves some empirical coefficients that are usually treated as universal constants.

Turbulent kinetic energy

$$\rho\frac{\partial(KE)}{\partial t}+\rho\frac{\partial}{\partial x_i}\left[v_iKE-\frac{ENUT}{PRT(KE)}\frac{\partial KE}{\partial x_i}\right]=\rho(P_k+\Gamma_b-EP) \tag{21}$$

Rate of dissipation

$$\rho\frac{\partial(EP)}{\partial t}+\rho\frac{\partial}{\partial x_i}\left[v_iEP-\frac{ENUT}{PRT(EP)}\frac{\partial EP}{\partial x_i}\right]=\rho\frac{EP}{KE}(C_{1e}P_k+C_{3e}\Gamma_b-C_{2e}EP) \tag{22}$$

$$ENUT=C_\mu C_d\frac{KE^2}{EP} \tag{23}$$

$$P_k=(ENUT)\frac{\partial v_i}{\partial x_j}\left(\frac{\partial v_i}{\partial x_j}+\frac{\partial v_j}{\partial x_i}\right) \tag{24}$$

$$\Gamma_b=\frac{-ENUT(g_i)\left(\frac{\partial\rho}{\partial x_i}\right)}{\rho(PRT(H))} \tag{25}$$

where the constants of the model are

C_μ = 0.5478
C_d = 0.1643
$C_\mu C_d$ = 0.0900
PRT(KE) = 1.000
PRT(EP) = 1.3140
C_{1e} = 1.4400
C_{2e} = 1.9200
C_{3e} = 1.000.

2.4. Spark ignition model development

During the combustion process preparation phase, the spark provided by the spark plug generates an energy equivalent to 115 mJ/spark. The ignition system is multi-spark, providing a spark every 20° of crankshaft turn.

An initial flame is formed around the first spark, from which the combustion gradually spreads to all the charge, depending on the spark front formed. As the combustion continues and is completed, the pressure inside the cylinder rapidly increases.

The combustion in piston engines is so complex that a satisfactory model has yet to be developed. One essential factor hindering the formulation of an appropriate theoretical approach is a lack of adequate knowledge regarding the nature of the turbulence-chemical reaction interactions. In the present study, the flame propagation is modeled using a two-zone model that accounts for the spark discharge energy and the effects of the flow turbulence on the kernel growth. After the spark discharge ignites the syngas–air mixture, a flame propagates outward from the spark plug.

The ignition kernel flame is very thin and separates the burned and unburned gas. The ignition kernel mass-burning rate is given by

$$\bar{m}_k=\frac{d(\rho_kV_k)}{dt}=\rho_uA_kS_t \tag{26}$$

The change in flame kernel internal energy is

$$\overline{Q}_{spk}=\left(\frac{\partial E}{\partial t}\right)_{cv}=m_k\frac{dU_k}{dt}+U_k\frac{dm_k}{dt}=m_k\frac{dU_k}{dt}+U_k\bar{m}_k \tag{27}$$

$$\overline{Q}_{mult-spk}=(\overline{Q}_{spk})(n_{spk}) \tag{28}$$

3. Solution methodology

3.1. Conditions of the analysis

(a) The thermodynamic system includes the cylinder and the combustion chamber.
(b) Half of the cylinder is simulated.
(c) The symmetry axis is located in the central part of the cylinder.
(d) The simulation includes the syngas combustion process.
(e) The chemical kinetics is modeled using the Arrhenius equation.
(f) The ignition system is multi-spark.
(g) The figures shown for each variable reflect the variation of the magnitude through time.
(h) The air–syngas feed mixture is premixed.
(i) The air–syngas ratio used is 1.1:1 (10% excess of air).
(j) The initial temperature of the mixture is 336 K.
(k) The initial pressure is 1 bar.
(l) Compression ratio = 10.35.
(m) Engine speed = 1500 rpm.

3.2. Numerical solution

The commercial CFD package, PHOENICS, with an IPSA algorithm, was used to simulate the syngas combustion process of SI engines. It is a finite volume program that uses a structured non-orthogonal grid and a staggered variable arrangement. The algorithm applies the finite volume to solve the transport equations set out. The CFD code in PHOENICS was used because of the ease with which the physical process can be elucidated using this code. The number of grids was fixed to a dimension of 6×5. The finest grid size in axial and radial directions is chosen as $\Delta z = 0.0293$ m and $\Delta y = 0.0128$ m, respectively.

All of the components are defined at the midpoints of the cell faces, whereas the scalar flow variables are defined at the cell centers. The IPSA algorithm was used for the scalar flow variables, where the solution was obtained iteratively starting from an initial condition.

The calculation domain was subdivided into zones corresponding to the existing physical discontinuities appearing in Fig. 1. In the present case, there are six zones in the axial direction (z) and five in the radial direction (y).

The number of grid points or finite volumes within each resulting subdivision of the domain was varied to ensure that the results were independent of the grid size. Numerical tests were also carried out to ensure that the results were independent of the number of iterations. Under relaxation was often necessary to achieve convergence, which was declared to have occurred when the cumulative residual for each of the conservation equations was less than 10^{-4}.

3.3. Spatial discretization

Fig. 1 shows the two-dimensional grid geometry in the yz-plane. The grid is uniform in both the y and z directions. Solutions for dependent variables (pressure, velocity, temperature, and con-

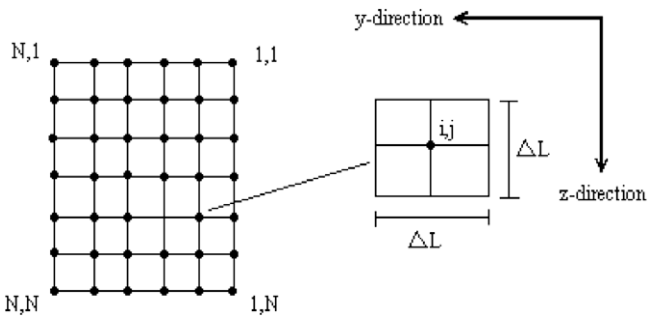

Fig. 1. Two-dimensional computational grid in the yz-plane.

centration for species in syngas) at nodes denoted in Fig. 1 are obtained. Each node is associated with a continuity cell of width and height ΔL for which the continuity and transport equations are solved. Here

$$\Delta L = \frac{L}{N-1} \tag{29}$$

where N is the total number of nodes in each direction.

3.4. Error analysis and uncertainty

Measured physical quantities are always subject to uncertainties. Uncertainty analysis was performed to verify the accuracy of the model. The uncertainties in the measurements are summarized in Table 2.

3.5. Methodology

The commercial CFD code in PHOENICS, with an IPSA algorithm, was used to simulate the syngas combustion process of the Diesel engine adapted to the Otto cycle. The algorithm applies the finite volume to solve the transport equations set out. The number of grid points was fixed to a dimension of 5×6. The CPU time per combustion process cycle was less than one second.

4. Model validation

In the literature, it is difficult to find models developed to simulate syngas combustion because syngas (a) is an unusual fuel, (b) is of limited commercial value, and (c) has a variable chemical composition that depends upon the type of residue used during gasification. These facts notwithstanding, the model developed for this work was compared to other models that evaluate syngas combustion in an ICE.

The model and numerical method were validated by comparing the calculated results to the models developed by Sridhar[27] and Peters [38], both of which use one spark during the syngas combustion.

Sridhar used a zero-dimensional model in conjunction with the wrinkled flame theory for flame propagation to understand the in-cylinder pressure behavior with time in a reciprocating ICE. The specifications and operating conditions used in the simulations of Sridhar and Peters were used in our model, as summarized in Table 3.

Fig. 2 shows the pressure variations obtained experimentally[27] along with the simulation data of the present study and from Sridhar. The two sets of simulation results are in satisfactory agreement. The error between the simulation data of the present study and from Sridhar in these measurements was around 8%.

The speed of the syngas–air mixture was also compared to the data of Sridhar (Fig. 3). The values obtained from the present study are in satisfactory agreement with the previous data. The error obtained with these measurements was 13.8% average.

Table 2
Uncertainty.

Parameters	Uncertainty (%)
Pressure (bar)	1.96
Speed (m/s)	1.28
Temperature (K)	1.20
Hydrogen (molar fraction)	3.92
Carbon monoxide (molar fraction)	1.52
Oxygen (molar fraction)	1.41
Carbon dioxide (molar fraction)	2.48
Water (molar fraction)	2.23

Table 3
Specification and operating conditions used in the simulation by Sridhar, Peters and this work (one spark).

H_2 (% by moles)	20.0
CO (% by moles)	15.0
CH_4 (% by moles)	2.5
CO_2 (% by moles)	14.0
H_2O (% by moles)	12.0
N_2 (% by moles)	36.5
Air/syngas ratio	1:1
Compression ratio	13.50
Number of cylinders	6
Engine speed (rpm)	1500
Inlet pressure (bar)	0.9
Inlet temperature (K)	300

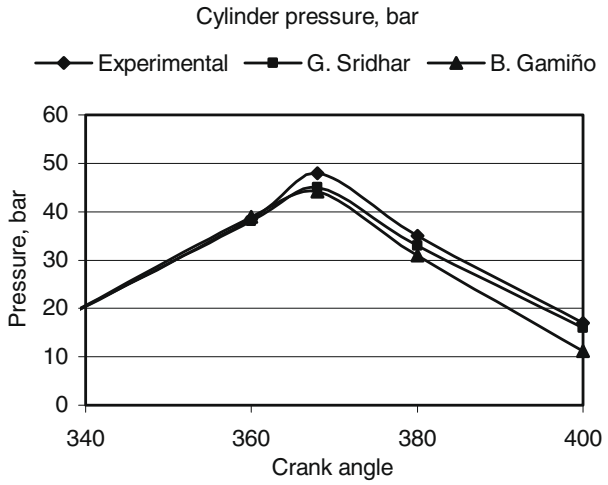

Fig. 2. Model results for cylinder pressure.

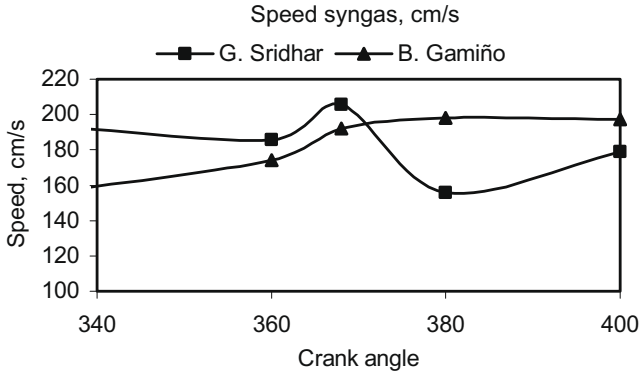

Fig. 3. Model results for syngas speed.

Fig. 4 shows the variation in temperature as a function of crank angle for the model of Peters as well as the present model. The error between the simulation data of the present study and from Peters in these measurements was around 8.6%.

5. Results and discussion

The results for the mass, energy, motion, and turbulence balances for the syngas combustion process inside the chamber and the bi-dimensional cylinder, expressed in polar cylindrical coordinates, were as follows.

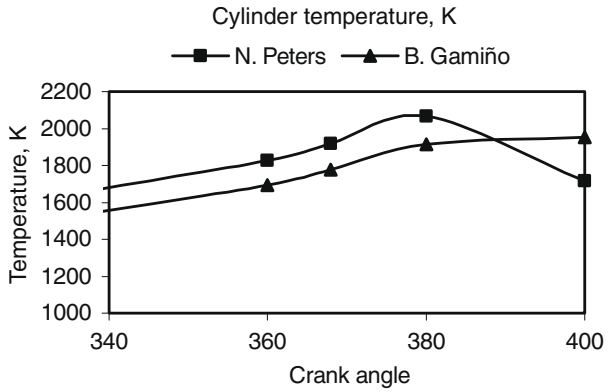

Fig. 4. Model results for cylinder temperature.

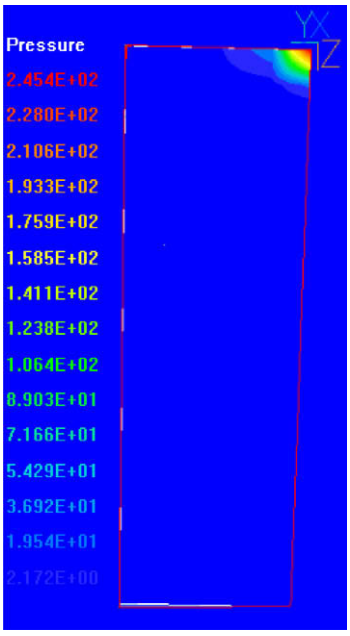

Fig. 5. Pressure profile (psi), from PHOENICS VR VIEWER, 3.5.

5.1. Pressure profiles

Fig. 5 shows the pressure variation through the chamber and the cylinder during the syngas combustion process. The pressure ranges from 245.3 psi (17 bar) at the beginning of the combustion to up to 31.5 psi (2.1 bar) at the end of the combustion on the bottom dead center.

The Fig. 6 shows the pressure variation with time for five radial zones, each of thickness 12.8 mm, moving out from the cylinder center from 0 to 64 mm. The greatest pressure change occurs in the innermost radial zone (0 to 12.8 mm), corresponding to the central part of the cylinder. During the first 4.5 ms, the pressure increases to 17 bar, after which it decreases to values of ~5 bar at 9 ms and ~1 bar at 13.5 ms.

5.2. Temperature profiles

Fig. 7 shows the predicted temperature of gases inside the cylinder as a function of time for the same five radial zones as in Fig. 6. In all radial zones, a maximum temperature of 1960 K is reached toward the end of the piston stroke. A temperature difference exists between the first and last burned gas zones. For syngas/air fuel mixtures, this difference is as large as 1000 K.

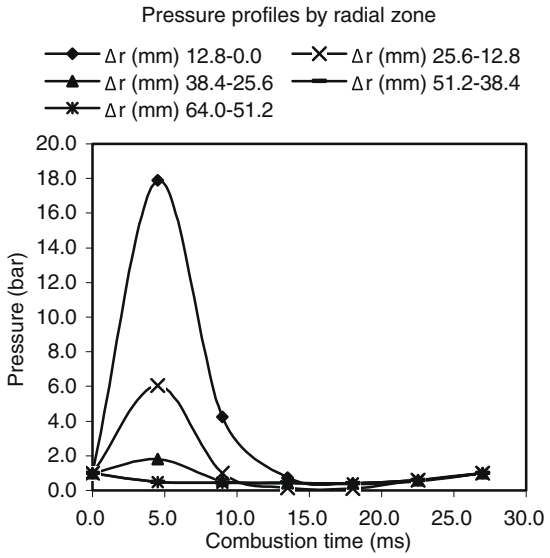

Fig. 6. Pressure profile (bar).

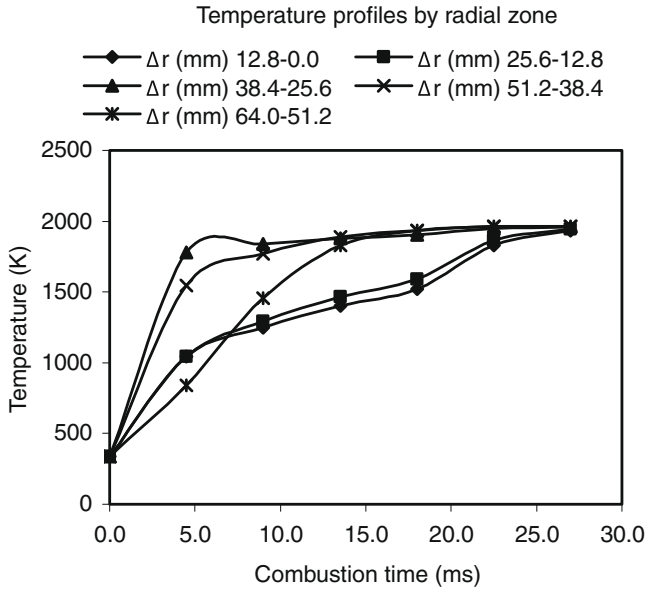

Fig. 7. Temperature profile (*K*).

Fig. 8 shows the predicted gas temperature variation. It can be seen that the temperature increases from 336 to 1960 K immediately after the syngas ignition process. The high temperatures reached practically from the beginning of the combustion process are the result of the multi-spark ignition system, which is necessary to compensate for the low flame speed of the hydrogen, carbon monoxide, and methane mixture.

The sixth zone in axial direction always has the highest temperature because, by the time the combustion-generated expansions of the following burn zones begin to compress the first zone, its temperature has already risen because of the release of chemical energy associated with the burned fuel mass.

5.3. Speed profile

Figs. 9 and 10 show the gas speed variations inside the chamber and the cylinder. The turbulent nature of the combustion process is reflected in the high speeds reached, which range from 51 m/s in

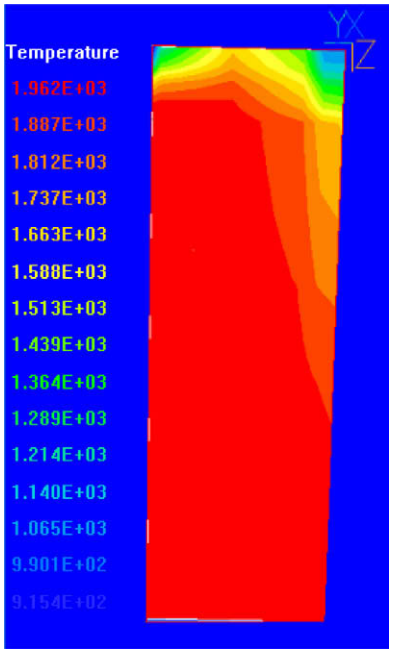

Fig. 8. Temperature profile (K), from PHOENICS VR VIEWER, 3.5.

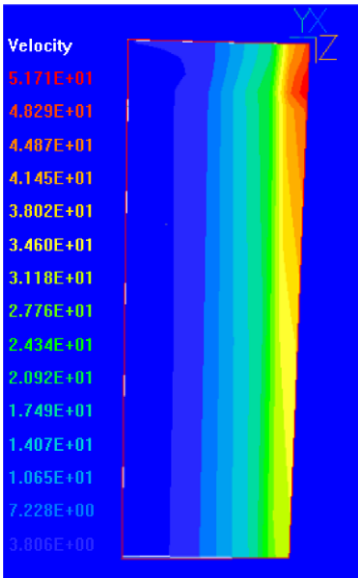

Fig. 9. Gas speed profile (m/s), from PHOENICS VR VIEWER, 3.5.

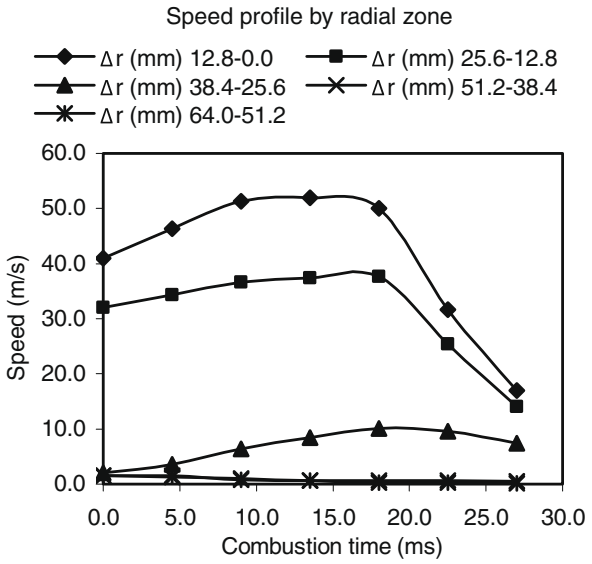

Fig. 10. Gas speed profiles (m/s).

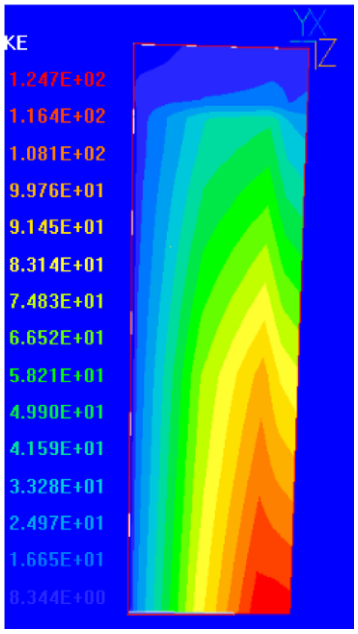

Fig. 11. Turbulent kinetic energy profile, from PHOENICS VR VIEWER, 3.5.

the central part to 3.8 m/s at the walls. The highest speeds are observed in the first two radial zones (0–12.8 mm and 12.8–25.6 mm); after 18 ms, the speed falls to below 20 m/s in both zones. For the radial zone of 51.2–64 mm (near the wall), the speed remains almost constant at ~3.8 m/s.

5.4. Turbulence intensity

5.4.1. Turbulent kinetic energy profile

The variations in turbulent kinetic energy inside the chamber and cylinder are shown in Figs. 11 and 12. In the central part of the cylinder, the energy ranges from 16.5 m^2/s^2 at the beginning of combustion to 124 m^2/s^2 at the end of combustion.

The turbulence intensity is highest in the radial zones spanning from 0 to 38.4 mm. The intensity increases after the first 18 ms.

5.4.2. Turbulent kinetic energy dissipation rate

Figs. 13 and 14 show the turbulent kinetic energy dissipation rate inside the chamber and cylinder. In the central part of the cylinder, this rate ranges from 3,487 m^2/s^3 at the beginning of combustion to 26,140 m^2/s^3 at the end of combustion. This extremely broad variation in the rate of dissipation reflects the complexity of the combustion process. In the two zones next to the wall of the cylinder (38.4–64.0 mm), the variations in the turbulent kinetic energy dissipation rate are minimal.

The turbulent kinetic energy dissipation rate increases with turbulent kinetic energy.

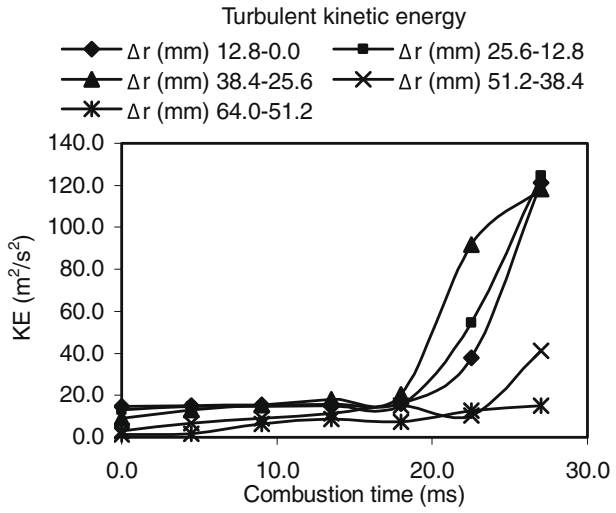

Fig. 12. Turbulent kinetic energy profile.

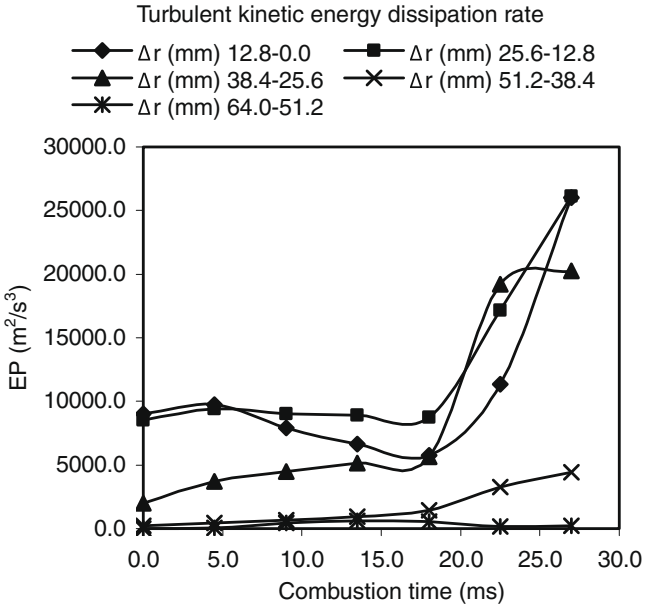

Fig. 13. Rate of dissipation profiles.

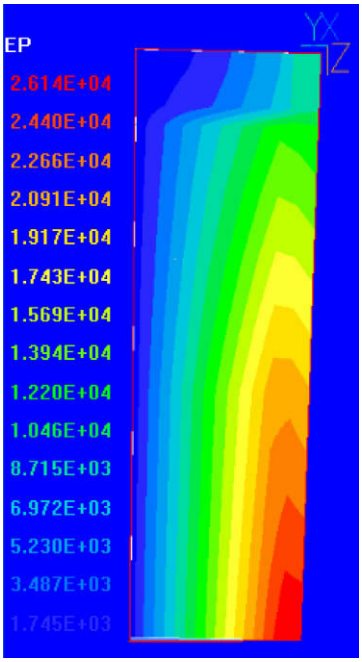

Fig. 14. Rate of dissipation profile, from PHOENICS VR VIEWER, 3.5.

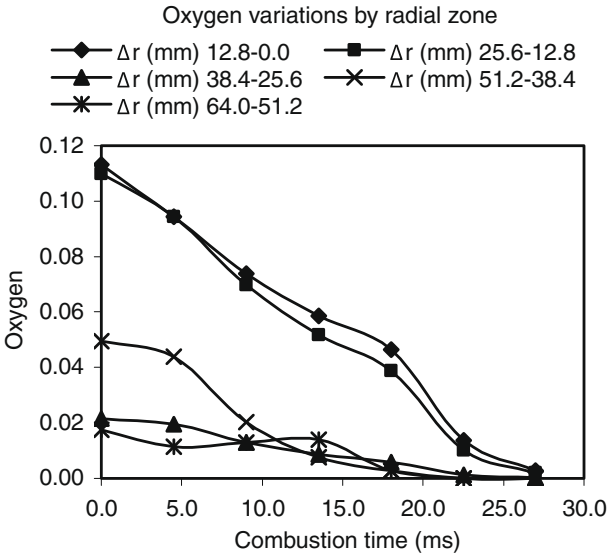

Fig. 15. Oxygen molar fraction.

5.5. Mean composition

The chemical composition at the commencement of combustion in percentages by moles is as follows: CO, 12.0%; H_2, 2.9%; CH_4, 2.4%; O_2, 11.0%; CO_2, 5.2 and N_2, 66.5%.

5.5.1. Oxygen molar fraction

As shown in Figs. 15 and 16 Oxygen falls from 0.11 at the beginning of combustion to close to 0 at the end of combustion. Significant decrements in the oxygen molar fraction are observed in the two radial zones at the center of the cylinder (0–25.6 mm). The combustion of the syngas is practically complete within 24 ms.

5.5.2. Hydrogen molar fraction

As shown in Figs. 17 and 18, the hydrogen falls from an initial value of 0.03 to close to 0 at the end of combustion. The hydrogen is consumed in the first half of the cylinder. The greatest decrements in the hydrogen molar fraction occur in the two inner radial zones (0–25.6 mm). After 22.5 ms, the hydrogen molar fraction undergoes minimal variation.

5.5.3. Carbon monoxide molar fraction

As shown in Figs. 19 and 20, the carbon monoxide falls from an initial value of 0.12 to close to 0 at the end of combustion. The greatest decrements in carbon monoxide molar fraction are observed in the two innermost radial zones (0–25.6 mm).

The molar fraction of reactants (O_2, H_2 and CO) decreases across the flame front (Figs. 15–20), and the temperature increases across the flame front (Figs. 7 and 8).

As the temperature rises in the reaction zone, the chemical reactions, which depend exponentially on temperature, increase until the reactants are consumed and their concentration decreases to zero.

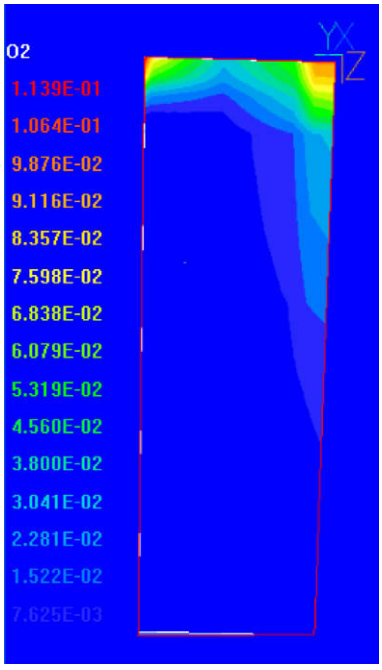

Fig. 16. Oxygen molar fraction, from PHOENICS VR VIEWER, 3.5.

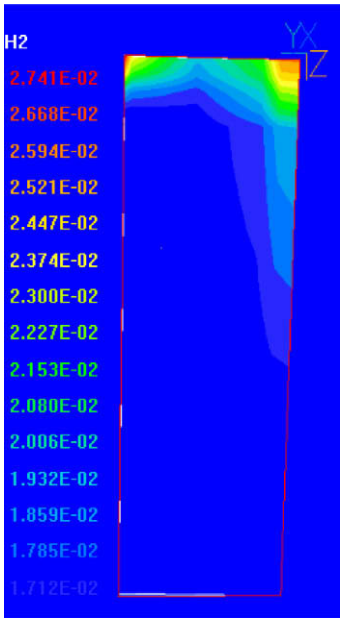

Fig. 18. Hydrogen molar fraction, from PHOENICS VR VIEWER, 3.5.

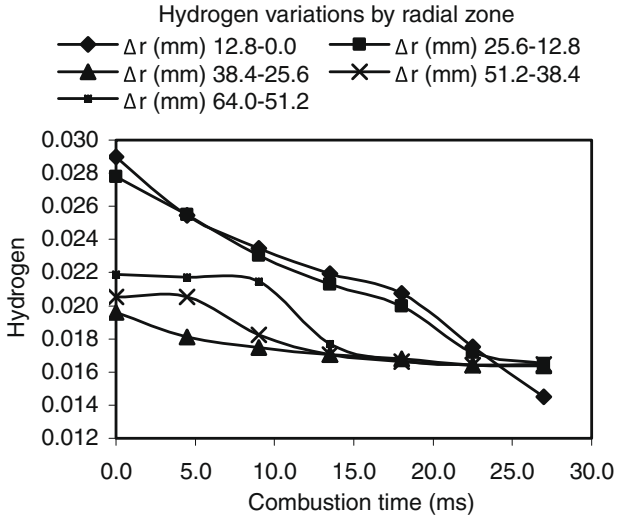

Fig. 17. Hydrogen molar fraction.

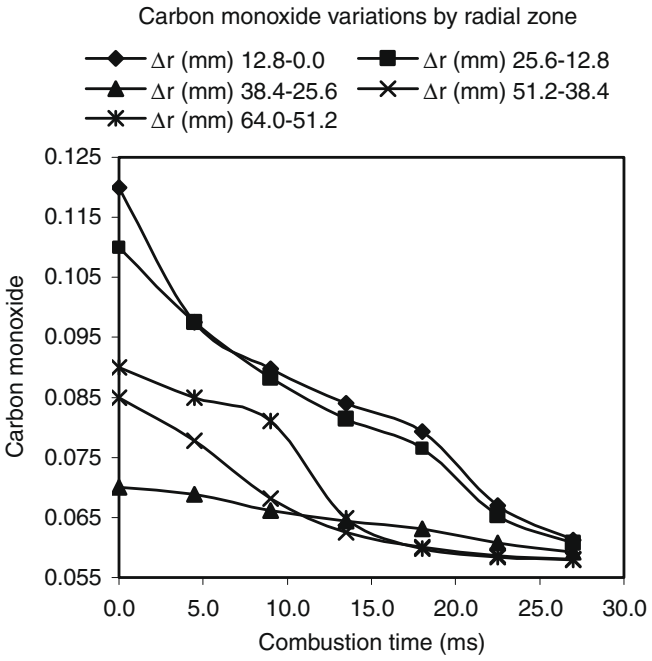

Fig. 19. Carbon monoxide molar fraction.

5.5.4. Water molar fraction

Interpretation of molecular transformations taking place in the course of the exothermic process of combustion is, thereupon, determined by chemical kinetics analysis of the transformation of reactants (O_2, H_2, and CO) onto products (CO_2 and H_2O) between their initial and final states established by the thermodynamic analysis.

Figs. 21 and 22 show the variations in the water molar fraction. The water molar fraction ranges from 0 to 0.11.

5.5.5. Carbon dioxide molar fraction

Figs. 23 and 24 show the variations of the carbon dioxide molar fraction, which ranges from 0.05 to 0.12. The evolution of the carbon dioxide molar fraction taking place in the course of the exothermic stage is as follows in Fig. 23.

5.6. Power variations

Fig. 25 shows the power variations for operation using syngas or Diesel as the fuel. The maximum power obtained for syngas operation ranges from 50 to 176 kW for engine speeds ranging from 1200 to 2300 rpm, whereas with Diesel, the power ranges from 77 to 260 kW for the same speed interval. At a given speed, the power of the system using syngas is ~68% of that of the Diesel operated system.

When the engine operates with Diesel or syngas, the engine performance curves are as follows in Fig. 25.

The minor power that is obtained in an operation using syngas is associated with the minor compression ratio (10.35 using syngas

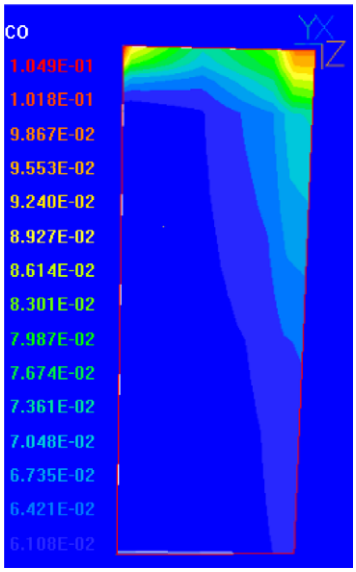

Fig. 20. Carbon monoxide molar fraction, from PHOENICS VR VIEWER, 3.5.

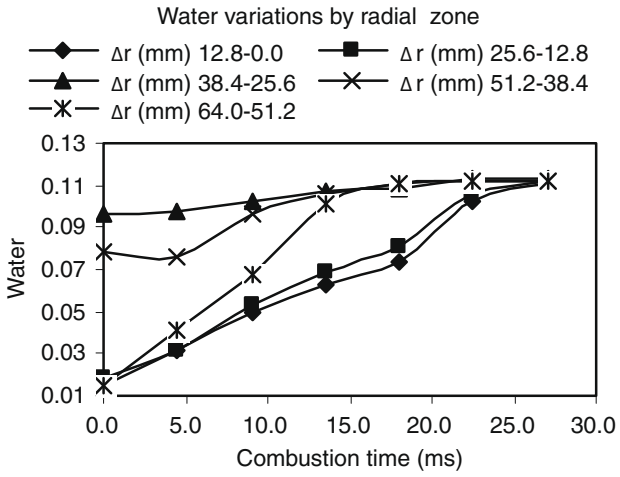

Fig. 21. Water molar fraction.

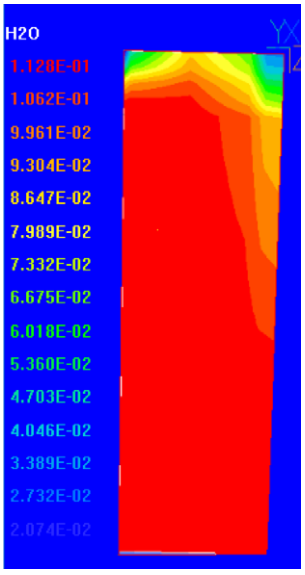

Fig. 22. Water molar fraction, from PHOENICS VR VIEWER, 3.5.

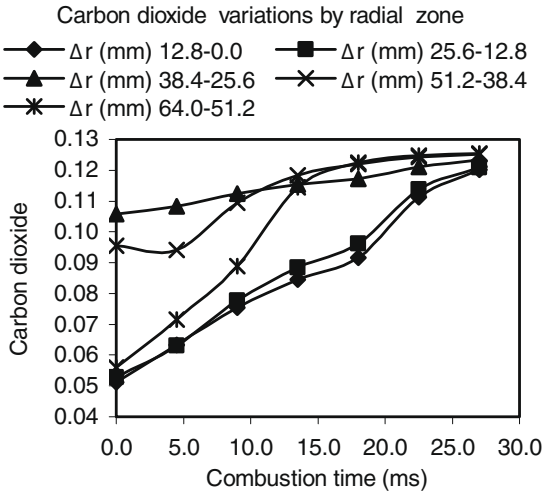

Fig. 23. Carbon dioxide molar fraction.

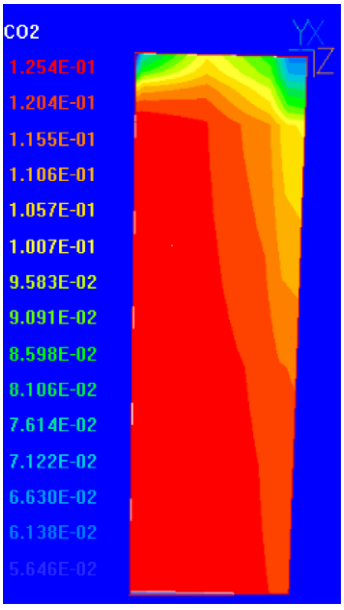

Fig. 24. Carbon dioxide molar fraction, from PHOENICS VR VIEWER, 3.5.

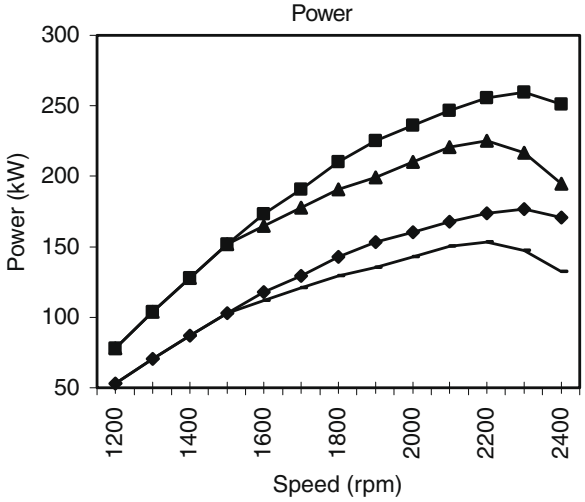

Fig. 25. Power variations.

and 17.25 using Diesel), and with the presence of substance diluents in the syngas (nitrogen and carbon dioxide), nevertheless, the present research demonstrates that the syngas is a fuel that can be used for the production of electricity using Diesel converted engines. The syngas will play an important role in the future global energy infrastructure for the generation of power.

6. Conclusions

We have simulated the syngas combustion process in an ICE using a mathematical model that includes the balances for the conservation of mass, energy, and reaction rates for the different chemically reactive species in syngas.

The simulations yielded predictions of the pressure, temperature, gas speed, and expected chemical composition profiles of the reactive substances and combustion products. The model and numerical method were validated by comparing the calculated results to those obtained using the models developed by Sridhar and Peters. In view of the success of these validations, we consider that the proposed model and calculation procedure are reliable.

The model was solved numerically using the CFD code in PHOENICS VR VIEWER, 3.5. The model employing 30 zones (6 zones in the axial direction and 5 zones in the radial direction) and 100 steps gave sufficiently accurate results to describe the combustion of syngas inside the chamber and cylinder. The number of grid points incorporated in the simulation did not affect the prediction results. The error is computed around 1 and 4% (Table 2). The central processing unit (CPU) time per combustion process cycle was less than one second. The thermal efficiency obtained was 32%.

The presented model is easy to use and is not computationally demanding. In addition, the model could easily be adapted to alternative fuel studies in SI engines. Finally, the model can be used to predict the parameters of syngas combustion inside the chamber and cylinder, which can be used for parametric studies.

Acknowledgement

The authors acknowledge the Engineering Institute of the National University of Mexico (UNAM), especially the macro-project "La Ciudad Universitaria y la Energía" (The UNAM Campus and the Energy), which provided the resources to carry out this research.

References

[1] Gong Changming, Deng Baoqing, Wang Shu, Su Yan, Gao Qing, Liu Xunjun. Combustion of a spark-ignition methanol engine during cold start under cycle-by-cycle control. Energ Fuels 2008;22:2981–5.
[2] Cho Gyubaek, Moon Gunfeel, Jeong Dongsoo, Bae Choongsik. Effects of internal exhaust gas recirculation on controlled auto-ignition in a methane engine combustion. Fuel 2009;2008:1042–8.
[3] Bayraktar Hakan. An experimental study on the performance parameters of an experimental CI engine fueled with diesel–methanol–dodecanol blends. Fuel 2008;87:158–64.
[4] Heywood JB. Combustion and its modeling in spark ignition engines. In: International symposium COMODIA; 1994. p. 1–15.
[5] Heywood JB. Internal combustion engine fundamentals. New York: McGraw-Hill; 1998.
[6] Yamin Jehad AA. Comparative study using hydrogen and gasoline as fuels: combustion duration effect. Int J Energ Res 2006;30:1175–87.
[7] Hu Tiegang, Wei Yanjv, Liu Shenghua, Zhou Longbao. Improvement of spark-ignition (SI) engine combustion and emission during cold start, fueled with methanol/gasoline blends. Energ Fuels 2007;21:171–5.
[8] Yanju Wei, Shenghua Liu, Hongsong Li, Rui Yang, Jie Liu, Ying Wang. Effects of methanol/gasoline blends on a spark ignition engine performance and emissions. Energ Fuels 2008;22:1254–9.
[9] Abu-Nada E, Al-Hinti I, Akash B, Al-Sarkhi A. Thermodynamic analysis of spark-ignition engine using a gas mixture model for the working fluid. Int J Energ Res 2007;31:1031–46.
[10] Boehman Andre' L, Corre Olivier Le. Combustion of syngas in internal combustion engines. Combust Sci Technol 2008;180:1193–206.
[11] Ma Fanhua, Wang Yu, Wang Junjun, Ding Shangfen, Wang Yefu, Zhao Shuli. Effects of combustion phasing, combustion duration, and their cyclic variations on spark-ignition (SI) engine efficiency. Energ Fuels 2008;22:3022–8.
[12] Ferguson C, Kirkpatrick A. Internal combustion engines: applied thermosciences. New York: Wiley; 2001.
[13] Heywood JB. Engine combustion modeling an overview. In: Combustion modeling in reciprocating engines. New York: Plenum Press; 1980.
[14] Naitoh K. Numerical simulation of the detailed flow and flame propagation in a homogeneous charge, Spark-Ignition Engine. In: International symposium COMODIA; 1990. p. 75–80.
[15] Hoffman Seth R, Abraham John. A comparative study of *n*-heptane, methyl decanoate, and dimethyl ether combustion characteristics under homogeneous-charge compression–ignition engine conditions. Fuel 2009;88:1099–108.
[16] Yusaf TF, Sye Hoe Fong, Yusoff MZ, Hussein I. Modeling of transient heat flux in spark ignition engine during combustion and comparisons with experiment. Am J Appl Sci 2005;2–10:1438–44.
[17] Sayin Cenk, Canakci Mustafa. Effects of injection timing on the engine performance and exhaust emissions of a dual-fuel diesel engine. Energ Conver Manage 2009;50:203–13.
[18] Saravanan N, Nagarajan G, Sanjay G, Dhanasekaran C, Kalaiselvan KM. Combustion analysis on a DI diesel engine with hydrogen in dual fuel mode. Fuel 2008;87:3591–9.
[19] Cordiner Stefano, Gambino Michele, Iannaccone Sabato, Rocco Vittorio, Scarcelli Riccardo. Numerical and experimental analysis of combustion and exhaust emissions in a dual-fuel diesel/natural gas engine. Energ Fuels 2008;22:1418–24.
[20] Huang Zuohua, Wang Jinhua, Liu Bing, Zeng Ke, Yu Jinrong, Jiang Deming. Combustion characteristics of a direct-injection engine fueled with natural gas-hydrogen mixtures. Energ Fuels 2006;20:1498–504.
[21] Saravanan N, Nagarajan G. Experimental investigation on a DI dual fuel engine with hydrogen injection. Int J Energ Res 2009;33:295–308.
[22] Sung Chih-Jen, Law Chung K. Fundamental combustion properties of H_2/CO mixtures: ignition and flame propagation at elevated pressures. Combust Sci Technol 2008;180:1097–116.
[23] Jie M, Yongkang SU, Yucheng Z, Zhongil Z. Simulation and prediction on the performance of a vehicle's hydrogen engine. Int J Hydrogen Energ 2003;28:7–83.
[24] Natarajan J, Lieuwen T, Seitzman J. Experimental and numerical investigation of strained laminar flame speeds for $H_2/O_2/N_2$ mixtures at elevated temperature. Combustion Meeting 2007; Paper No. A02.
[25] Ono Ryo, Oda Tetsuji. Measurement of OH density and gas temperature in incipient spark-ignited hydrogen–air flame. Combust Flame 2008;152:69–79.
[26] Yusaf TF, Yusoff MZ, Hussein I, Fong SH. A quasi one-dimensional simulation of a 4 stroke spark ignition hydrogen fuelled engine. Am J Appl Sci 2005;2–8:1206–12.
[27] Sridhar G, Paul PJ, Mukunda HS. Zero-dimensional modeling of a producer gas-based reciprocating engine. In: Proc. IMechE 2007; vol. 220, DOI: 10.1243/09576509JPE265.
[28] Rakopoulos CD, Rakopoulos DC, Kyritsis DC. Development and validation of a comprehensive two-zone model for combustion and emissions formation in a DI diesel engine. Int J Energ Res 2003;27:1221–49.
[29] Moriyoshi Y. Experimental evaluation of calculation models used in in-cylinder flow field computations. In: Internal symposium COMODIA; 1994. p. 553–8.
[30] Sahin Zehra, Durgun Orhan. Multi-zone combustion modeling for the prediction of diesel engine cycles and engine performance parameters. Appl Thermal Eng 2008;28:2245–56.
[31] Tan Zhichao, Reitz Rolf D. An ignition and combustion model based on the level-set method for spark ignition engine multidimensional modeling. Combust Flame 2006;145:1–15.
[32] Patrick Parke, Stanley Clark, Walter Wandeler. Biomass Producer fueling of internal combustion engines. Kansas State University, EE.UU; 1981.
[33] Bird RB, Stewart WE, Lightfoot EN. Fenómenos de transporte. México: Reverté; 1980.
[34] Mura Arnaud, Robin Vincent, Champion Michel. Modeling of scalar dissipation in partially premixed turbulent flames. Combust Flame 2007;149:217–24.
[35] Grimsmo B, Magnussen FB. Numerical calculation of turbulent flow and combustion in a Otto engine using the Eddy dissipation concept. In: International symposium COMODIA; 1990. p. 65–73.
[36] Tabet-Helal F, Sarh B, Menou A, Gö Kalp I. A comparative study of turbulence modeling in hydrogen-air nonpremixed turbulent flames. Combust Sci Technol 2006;178:1887–909.
[37] Michel Jean-Baptiste, Colin Olivier, Veynante Denis. Modeling ignition and chemical structure of partially premixed turbulent flames using tabulated chemistry. Combust Flame 2008;152:80–99.
[38] Peters N. Four lectures on turbulent combustion. Germany: Institut fur Technische Mechanik; 1997.
[39] Soma S, Ramírez AI, Hagerdorna J, Savelieva A, Aggarwal SK. A numerical and experimental study of counterflow syngas flames at different pressures. Fuel 2008;87:319–34.
[40] Akkerman V'yacheslav, Bychkov Vitaly, Eriksson Lars-Erik. Numerical study of turbulent flame velocity. Combust Flame 2007;151:452–71.
[41] Zhao X, Matthews RD, Ellzy JL. Numerical simulations of combustion in SI engines: comparison of the fractal model to the coherent flame model. In: International symposium COMODIA; 1994. p.157–62.